Comparison of Experimental and Computational Values of Flame Radiation

D. S. Babikian* and D. K. Edwards†
University of California, Irvine, California

Procedures for making bandpass-filtered total radiometer measurements are described, and comparisons of the readings are made with soot and gas-band models of a spray-atomized flame. Three flames with different soot contents were examined. Liquid fuels used were an iso-octane-tetralin mixture, a Suntech-3 aircraft fuel blend, and petroleum JP-4. These were sprayed by a Parker-Hannifin twin-fluid 60-deg hollow-cone nozzle into swirling combustion air and dilution air flowing in an 80-mm-diam duct at atmospheric pressure. Bandpass-filtered radiometric observations at an axial location of $x/R = 4.75$ are reported. The readings are compared to predictions made using the exponential wideband model for gas radiation with added provision for the presence of soot at its own temperature. The comparisons show that the discrepancy between the experimental readings and the model predictions is within 3%.

Nomenclature

A = band absorption, m^{-1}
B = Planck function, $W/m^2\ m^{-1}$
c = speed of light, m/s
D = diameter of flame, m
h = Planck constant, J · s
I = radiant intensity, W/m^2 sr
k = Boltzmann constant, J/K
K = mass absorption coefficient, m^2/kg
L = path length, m
n = wavelength decay exponent
n = number of filters
q = radiant flux, W/m^2
r = local radius, m
R = combustor radius, m
t = optical depth
T = temperature, K
U = mean axial velocity, m/s
x = axial location in combustor, m
X = mole fraction
α = integrated intensity, $m^{-1}/kg\ m^{-2}$
β = line width parameter
γ = ratio of $K_a(\lambda_P)/K_o$
δ = rms discrepancy
ϵ = emissivity
η = line width to spacing ratio
λ = wavelength, m
ν = wavenumber, m^{-1}
π = 3.14159 . . .
ρ = density, kg/m^3
τ = transmissivity
ω = bandwidth parameter, m^{-1}

Subscripts

a = absorber, absorption
c = calibration
D = detector
E = electronic band
g = gas
h = head of the band
k = kth band
M = heat flux meter
o = reference value, observed
p = predicted
P = pyrometer
s = soot

Presented as Paper 86-1319 at the AIAA/ASME 4th Thermophysics and Heat Transfer Conference, Boston, MA, June 2-4, 1986; received Dec. 19, 1986; revision received March 25, 1987.

*Research Assistant, Department of Mechanical Engineering. Student Member AIAA.

†Professor and Associate Dean, Department of Mechanical Engineering. Associate Fellow AIAA.

Introduction

HEAT radiation from flames is a significant fraction of the total heat flux on the liner of a gas turbine combustor.[1,2] The radiation is emitted by the hot gases of the combustion products and the soot particles generated in fuel-rich regions of the flame.[3,4] The spectra in the visible and ultraviolet regions are generally due to transitions of electrons from one configuration to another.[5] The large part of the energy radiated by flames lies in the infrared. The gas radiation is due to changes of vibrational and rotational energy of the molecules. Hot soot particles emit in continuous spectra determined by their temperatures and spectral absorption coefficient.

Scaling up the measurements of thermal radiation from laboratory combustor flames to determine the radiative heat flux in flight combustors requires knowledge, for each combustor, of the effective radiant temperature and the optical thickness of soot particles, as well as the gas composition and temperature. It appeared that filtered total radiometer measurements along with gas sampling could be used to obtain the needed information.

Thus, the objectives of this paper were: 1) to demonstrate proper procedures for making bandpass-filtered total radiometer measurements on a combustor, 2) to see how well such measurements would agree with predictions based on existing engineering correlations of gas and soot radiation, and 3) to discover how to use the measurements to indicate effective radiant temperatures of the gas and soot and the soot loading. Accordingly, commercial filters and radiometers were surveyed and selected. Bandpass-filtered total radiometer and optical pyrometer measurements were made from a spray-atomized gas turbine burner fired into atmospheric pressure dilution air swirling in an 80-mm duct,[6] as shown in Fig. 1. Three flames with different soot loadings were examined at $x/R = 4.75$. Spatially resolved nonintrusive laser soot countings were made by our colleagues.[7] The gas composition field for each fuel was mapped with a sampling probe connected to gas analyzers.

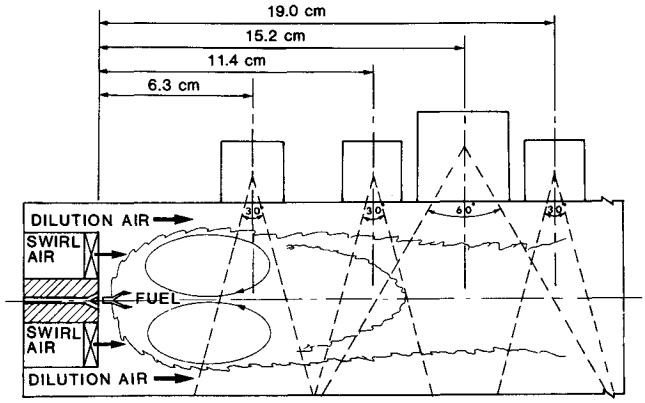

Fig. 1 Schematic of combustor.

In what follows, the filter selection, calibration procedures, and filtered radiometer mounting on the combustor are briefly described. Then, data interpretation and the experimental results are discussed. It is shown that the gas temperature can be assigned a value that is insensitive (± 50 K) to soot loading and temperature. Effective soot temperature and optical depth are indicated by a sharp minimum in rms discrepancy between a set of filter readings and predictions and confirmed by the optical pyrometer reading. With the gas and soot temperatures and soot optical depth assigned, the rms discrepancy is shown to be approximately 3%.

Experimental Approach

Filter and Radiometer Selection

Water-cooled and gas-purged radiometers (Medtherm Model 64P-05-24) with a 15 deg half-angle field of view were used. With the standard sapphire window on the detector, the radiometer detects radiation in the 0.2–7.0-μm spectrum. Figure 2 shows the spectral transmissivity of the sapphire window and indicates the spectral locations of gas bands and 2000 K soot emission. Six commercial filters were selected to be used individually or in pairs, with the goal of distinguishing the radiation from individual gas bands, as well as isolating short-wavelength soot radiation. The six filters were four from Corion Corporation (Models LS1000, RL1500, RL3500, RS3500), one from Oriel Corporation (Model 58010), and one from OCLI (astronomy filter J). In addition to these filters, a Pyrex, quartz, or sapphire window was used as needed to complete a pair. Pairs were used to reduce reradiation from filter heating.

Table 1 shows two sets of filter selections. Figures 3 and 4 display the transmittance spectra for the second set of the filters. The spectra were obtained with Cary 17D and Perkin Elmer 283 spectrophotometers.

Table 1 Filters and calibration constants

	Set 1 for cases 1 and 2		Set 2 for case 3	
Filter no.	Filter	Calibration constant[a]	Filter	Calibration constant
F0	Pyrex + Astronomy Type J	0.400	Astronomy Type J	0.400
F1	Quartz + LS1000	0.414	LS1000	0.440
F2	RL1500 + LS1000	0.410	RL1500 + LS1000	0.440
F3	Quartz + RS3500	0.395	RS3500	0.435
F4	RL1500 + RS3500	0.410	RL1500 + RS3500	0.445
F5	58010 + RL3500	0.498	58010 + RL3500	0.540
F6	Sapphire + RL3500	0.526	RL3500	0.550
F7	Sapphire + Sapphire	0.470	Sapphire	0.468

[a]Constants for cases 1 and 2 were obtained with the purge air on.

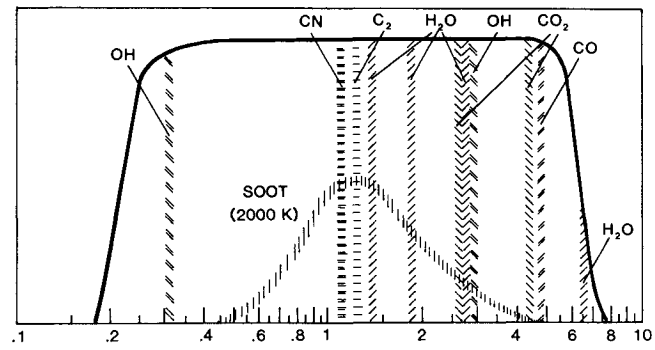

Fig. 2 Spectral layout of radiating gas bands and soot.

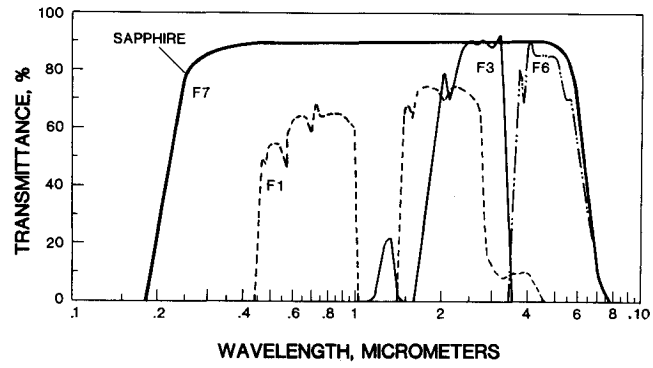

Fig. 3 Spectra of individual filters.

Filter F0 passed wavelengths between 1.1 and 1.4 μm. Figure 2 shows this region to include radiation from soot and the C_2 (Phillips) and CN (red) band systems.[8,9] Filters F1 and F2 were to isolate short-wavelength soot radiation. An excess in the reading of F1 over F2 after allowances for their transmissivities would indicate radiation at wavelengths shorter than 1.0 μm. Filters F3 and F4 were to distinguish midwavelength soot and gas radiation, mainly the H_2O and CO_2 bands at 2.7 μm. Filter F5 was to isolate the strong fundamental CO_2 band at 4.3 μm and that of CO at 4.7 μm. Filter F6 showed additionally the portion of 6.3-μm water vapor band passing through the sapphire window of the radiometer.

Filtered Radiometer Calibration

The radiometer readout settings were calibrated by the manufacturer to indicate πI outside the radiometer window. Here I is the total (spectrally integrated) radiant intensity (W/m^2sr) averaged over the field of view. The quantity πI will be termed "flux" in this paper. The calibration so made accounts not only for the inherent response of the detector but also for the total transmissivity of the sapphire window for the source radiation. With the addition of a 4-mm stop (above the inner sapphire window to reduce the field of view of the radiometer) and filters, as shown in Fig. 5, the manufacturer's calibration becomes moot. Accordingly, each filter or filter pair was calibrated by having the radiometer view a blackbody cavity through the filter.

A computer program, making use of the filter band model, predicted the net radiant flux at the surface of the detector within the inner sapphire window. In this calculation, the detector was assumed black, the filters were assumed to be at the radiometer temperature, and interreflections were neglected. A linear relationship was used to convert an indicated flux to the net flux at the detector,

$$q_D = (q_D/q_M)_c \cdot q_M \qquad (1)$$

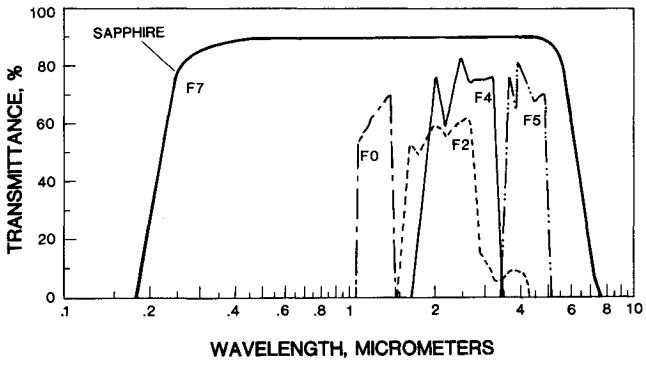

Fig. 4 Spectra of paired filters.

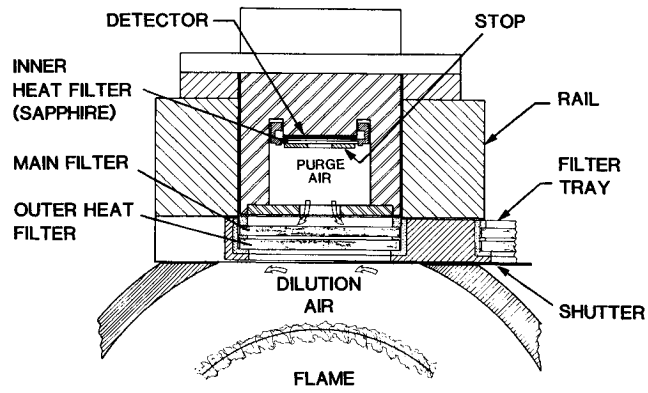

Fig. 5 Radiometer mounting details.

where subscript c denotes calibration, M a heat flux meter reading, and D the net flux at the detector. The ratio $(q_M/q_D)_c$ for each filter is its calibration constant.

If the computer model and the filter band models were totally accurate, and the detector truly black and nonselective, one would expect all the calibration constants to be identical, all equal to the area of the added inner stop divided by the original active area and the total transmissivity of the sapphire radiometer window at the temperature used by the manufacturer to calibrate. Table 1 shows the calibration constants found. A tendency appears for the short-wavelength filter calibration constants to be somewhat lower than those for the long-wavelength filters. Note that the filters used in set 1, although having the same designations, were in many cases, duplicates. Where more than one filter with the same model number was used, each had its spectral transmittance measured and modeled. The differences in calibration constants between sets 1 and 2 for filters F2, F4, and F5 emphasize the need for recalibration whenever new filters are put into service.

Additionally, a purge-air effect was found on the radiometer readout. A zero shift occurs when purge air is turned on, and allowance was made for the shift.

Flame Radiation and Gas Composition Measurements

The UCI combustor used, pictured in Fig. 1, has been described previously, e.g., in Refs. 6 and 7. A Parker-Hannifin twin-fluid injector sprays at 60 deg angle into dilution air flowing in an 80-mm duct. Dried dilution airflow is in the outer annulus. Swirl air is 62.5% of the total dilution air and enters at 60 deg from the axis. Dilution plus swirl air is maintained constant at 4.5×10^{-2} kg/s (80 scfm). Fuel flow is controlled to give the desired equivalence ratio of stoichiometric air to dilution "plus swirl" air, and the atomizing nozzle air-fuel ratio is set as desired. Note that the equivalence ratio cited does not include the nozzle air. Table 2 shows the fuels, equivalence ratios, and nozzle air-fuel ratios selected to give a clean flame, a slightly sooty flame, and a very sooty flame. Note that the nozzle air for the JP-4 flame was halved to enhance soot formation.

Table 2 Combustion conditions

Parameter	Case 1	Case 2	Case 3
Fuel liquid	Iso-Tet[a]	Suntech-3	JP-4
H-C ratio	2.128	1.898	2.031
Equivalence ratio	0.5	0.3	0.3
Nozzle air-fuel ratio A/F	3.0	3.0	1.5
Air preheat	100°C	100°C	100°C

[a]92% iso-octane and 8% tetralin by volume.

To define the radiative boundary conditions, the combustor wall was painted with Pyromark 2500 high-temperature black paint, cured according to instructions.

Figure 5 shows the radiometer and filter setup. The filters, which were held in trays that could be inserted or removed from the radiometer rail, were 25 mm in diameter and were located within 4 mm of the 6-mm-diam radiometer mouth. Thus, the filters completely filled the field of view of the radiometer. A 1-mm air gap separated filters in a pair, and a bright aluminum shutter was inserted to obtain zero readings before and after each observation. The radiometer outputs were monitored on the digital display of the Medtherm four-channel (Model H-201) heat flux meter. During each filter reading and shutter zero reading, the linear analog output of the heat flux meter was recorded for about 1 min using a multichannel strip chart recorder.

For each of the runs, gas composition was mapped using a hot-water-cooled extractive probe connected to four instruments: a Scott Model 150 oxygen analyzer, two Beckman Model 215B IR analyzers for CO_2 and CO, and a Scott Model 215 heated total hydrocarbon analyzer. Nitrogen oxides were not sampled, because their small concentrations have little effect on flame radiation from the burner used. Figure 6 shows the mapping for each of the fuels used.

Data Interpretation

Optical Beam Length

Top-hat profiles were fit to the composition curves by equating the first and second moments. The O_2 and CO_2 profiles were used to set the flame radius at a station. With this

Table 3 Top-hat compositions at x = 19.0 cm

	Mole fractions					
	Case 1		Case 2		Case 3	
	Iso-Tet D = 5.066 cm		Suntech-3 D = 4.614 cm		JP-4 D = 5.380 cm	
Species	Dry basis	Wet basis	Dry basis	Wet basis	Dry basis	Wet basis
CO_2	0.1014	0.0880	0.1068	0.0933	0.1086	0.0939
CO	0.0458	0.0398	0.0456	0.0399	0.0401	0.0346
CH_4	0.0050	0.0043	0.0005	0.0004	0.0008	0.0007
O_2	0.0345	0.0299	0.0440	0.0385	0.0274	0.0237
H_2O	—	0.1319	—	0.1260	—	0.1361

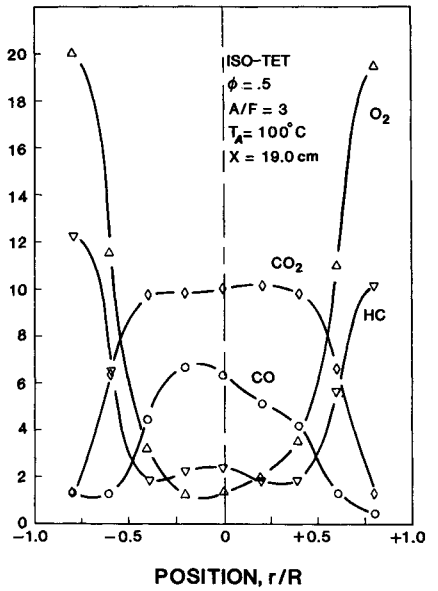

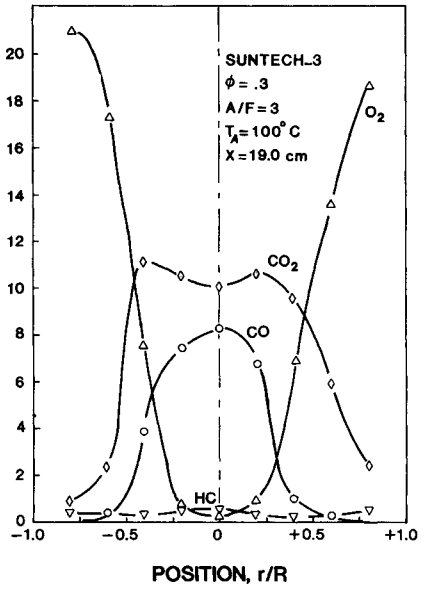

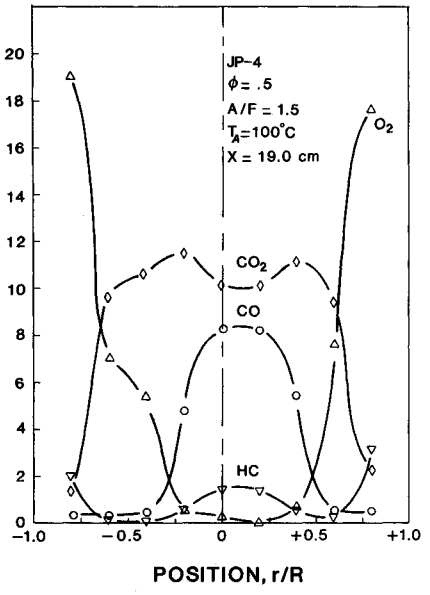

Fig. 6 Gas composition profiles.

radius prescribed, the first moments set the mole fractions in the flame. For example, at $x = 19.0$ cm and for JP-4, corresponding to the profiles shown in Fig. 6b, the core radius was taken as 2.69 cm. Thus, the flame diameter was 5.38 cm out of the 8.0-cm-diam duct. The mean beam length viewed by the radiometers was taken as the core diameter.

Gas Composition

The core-averaged dry-basis gas composition was used to infer core-averaged H_2O composition by carbon, hydrogen, and oxygen balances in which it was assumed that the carbon in CO_2, CO, and hydrocarbons (taken as CH_4) came from the liquid fuel, and the fuel hydrogen not appearing as CH_4 was present as H_2O. Note that the hydrocarbon mole fractions at the axial location of the measurements were low, and the correction for unburned fuel hydrogen was slight. The oxygen balance indicated that the air entrainment and, thus, all mole fractions were expressed on a wet basis. Table 3 shows the core-averaged mole fractions of the major species for the three runs at $x = 19.0$ cm.

Computer Model

The exponential wideband model described in Ref. 10 is used. The model for a given band is defined by a bandwidth parameter ω, a line width parameter β, and the integrated band intensity α. The methodology and data necessary to make band calculations have been well described in the literature. From the mole fractions, the pressure, and a prescribed value of temperature, the absorber-density-path-length product $\rho_a L$ was found, and the maximum optical depth for the kth absorption band was calculated.

$$t_{H,k} = \alpha_k \rho_a L / \omega_k \tag{2}$$

With values of $t_{H,k}$ and a ratio of mean line width to spacing, η_k, the band absorption A_k and bandwidth $\Delta\nu_k$ were found for each of the bands.

The gas band transmissivity was calculated from band absorption as recommended in Ref. 11,

$$\tau_g = (t_{H,k}/A_k)(\mathrm{d}A_k/\mathrm{d}t_{H,k}) \tag{3}$$

Provision for soot was made with a prescribed optical thickness and temperature. The absorption coefficient of soot was assumed to vary as

$$K_a = K_o(\lambda_o/\lambda)^n \tag{4}$$

where wavelength-decay exponent n is approximately 0.8 in the 1.3-3.0-μm wavelength region.[12] For convenience in calculations, the reference wavelength λ_o was selected to be 2.0 μm, and the amount of soot present was described by the optical depth at $\lambda = 2.0$ μm, $t_s = \rho_s K_o L$. The spectral emissivity of soot is, accordingly,

$$\epsilon_\lambda = 1 - \exp\,[-t_s(\lambda_o/\lambda)^n] = 1 - \tau_s \tag{5}$$

Since two distinct temperatures were involved, one for the soot and the other for the gas, a mean source intensity was computed at each wavelength of integration

$$\bar{B}(\lambda) = \frac{t_{s\lambda}B(\lambda,T_s) + t_{g\lambda}B(\lambda,T_s)}{t_{s\lambda} + t_{g\lambda}} \tag{6}$$

where the optical depth of the soot is $t_{s\lambda} = t_s\,(\lambda_o/\lambda)^n$ and the equivalent optical depth of the gas $t_{g\lambda}$ is found from

$$t_{g\lambda} = \ell n(1/\tau_{g\lambda}) \tag{7}$$

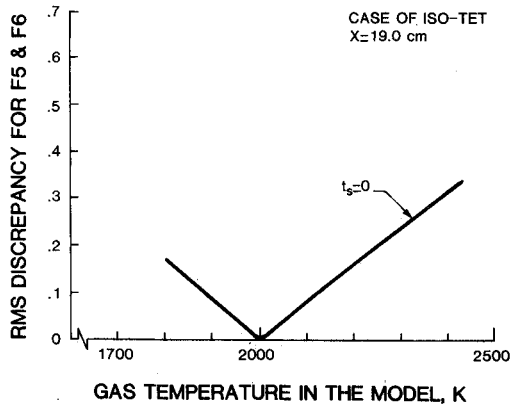

Fig. 7 Effect of gas temperature on rms discrepancy, Iso-Tet.

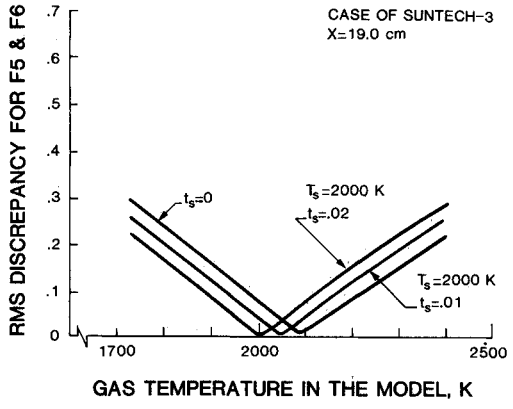

Fig. 8 Effect of gas temperature on rms discrepancy, Suntech-3.

The symbol $B(\lambda,T)$ denotes the Planck function

$$B(\lambda,T) = \frac{2\pi hc^2\lambda^{-5}}{\exp(hc/\lambda kT) - 1} \tag{8}$$

The measure of goodness of fit of the model predictions to the filtered radiometer observations was taken to be the rms discrepancy

$$\delta = \sqrt{\frac{1}{N}\sum_{i=1}^{N}\left(\frac{q_p - q_o}{q_o}\right)_i^2} \tag{9}$$

where N is the number of filters considered and q_p and q_o are, respectively, the predicted and observed heat fluxes at the detector.

Optical Pyrometer Measurement

A disappearing filament optical pyrometer (Pyrometer Instrument Co., Model 95) was used to measure the apparent soot temperature $T_{s,o}$ of the Suntech-3 and JP-4 flames. The red filter in the instrument cuts off short wavelengths. Approximating the product of the pyrometer spectral filter transmittance and the spectral response of the observer's eye to be a delta function at $\lambda = \lambda_P = 0.62$ μm allows the true temperature T_s to be expressed as a function of ϵ_λ and thus optical depth t_s through Eq. (5),

$$T_s = \frac{hc/\lambda k}{\ell n\,\{1 + \epsilon_\lambda[\exp(hc/\lambda kT_{s,o}) - 1]\}}, \quad \lambda = \lambda_P \tag{10}$$

Results and Discussion

The Iso-Tet flame with preheated air was pale blue, and the laser particle counter indicated no soot.[6,7] The Suntech-3 flame with normal nozzle air-fuel ratio was pale yellow. The flame for JP-4 with reduced nozzle air was a very bright yellow, and a high laser particle count was observed. Initially, the filters selected were as shown in Table 1, set 2, and the readings for filters F3 and F7 appeared high in comparison to the other readings. At first, it was thought that radiation was being contributed by the C_2 Phillips band system not included in the correlations of Ref. 10. To check this possibility, filter F0 was procured, and a zero reading was observed for the Iso-Tet flame, eliminating the possibility. It was then concluded that single-filter heating and reradiation was contributing to the high readings. Accordingly, readings were repeated for Iso-Tet and Suntech-3 using paired filters as shown in Table 1, set 1. Furthermore, to reduce the effect of filter heating on the readings, a shutter zero reading was taken before and after each filter reading.

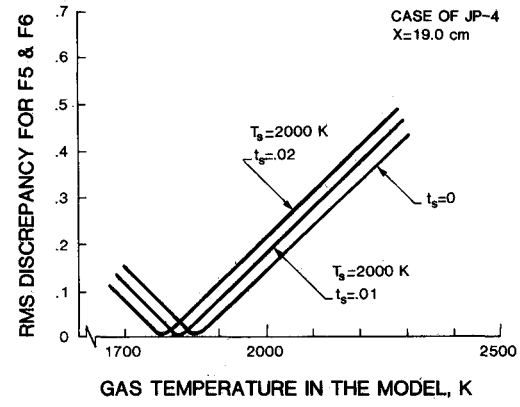

Fig. 9 Effect of gas temperature on rms discrepancy, JP-4.

Table 4a Comparison of experimental readings with computer model predictions (case 1, Iso-Tet, at x = 19.0 cm)

Filter no.	Experimental readings, W/m^2, q_D ($\pm$ 50)	Predicted values, W/m^2, q_D	Discrepancy, %
F0	0	0	—
F1	1840	2030	+ 10
F2	1780	1880	+ 5
F3	2910	3050	+ 5
F4	2830	2800	− 1
F5	7170	7170	0
F6	8120	8110	0
F7	11380	10850	− 5
Total spectrum	—	19020	—
rms (F3-F7)	—	—	3

Note: Inputs for gas and soot: T_g = 2000 K, t_s = 0, (T_s irrelevant).

Figure 7 shows the filters F5 and F6 rms discrepancy between the Iso-Tet readings and predictions as a function of T_g in the model. A sharp minimum in the two-filter rms discrepancy is seen to occur in the vicinity of T_g = 2000 K. Table 4a shows the individual filter discrepancies when model predictions are made using this temperature.

Figures 8 and 9 show similar plots for the Suntech-3 and JP-4 flames, respectively. The figures show that the indicated gas temperature is insensitive to the amount of soot included in the model because readings F5 and F6 are affected strongly by T_g but not by T_s and t_s. Figure 10 shows seven-filter rms discrepancy vs soot temperature at the best T_g for three values of t_s. Sharp minima can be seen, one for each soot loading assignment. The locus of these minima is plotted on the right side of Fig. 11. On the left side of the figure, the value of the rms discrepancy at each local minimum is plotted. The local minima have a minimum at a soot loading of t_s = 0.0105 and a soot temperature of T_s = 2035 K.

To test the sensitivity of the results to mean beam length (or gas concentration since it is the product of the two that matters) the mean beam length was varied $\pm$ 10%, and the

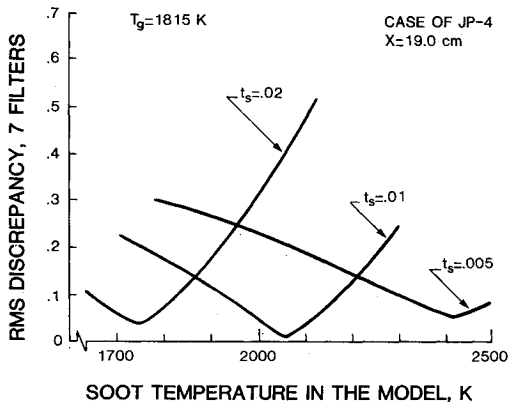

Fig. 10 Effect of soot temperature on rms discrepancy.

values of T_g, T_s, t_s, and δ were recomputed. The value of T_g was affected by $\mp 3\%$, and the values of soot temperature and optical depth were unaffected. The rms discrepancy δ was lowest for the assigned base value of mean beam length shown in Table 3, supporting the value chosen on the basis of the first and second moments of the gas composition profiles.

Also shown on the right side of Fig. 11 is T_s vs t_s, indicated by Eq. (10) based on the optical pyrometer reading. In plotting T_s vs t_s based on the optical pyrometer reading, it is necessary to assign γ equal to the ratio of K_a at $\lambda = 0.62$ μm to K_o at $\lambda = 2.0$ μm. The ratio $\gamma = 2.0$ was selected based on the dispersion model of Tien and Lee.[12] The location of the optical pyrometer curve is rather insensitive to the assignment of γ, and the locus of minima is quite insensitive to the value of n in Eq. (4). If γ is increased from 2.0 to 2.5, T_s goes down by 50 K and t_s up by 10%. With $\gamma = 2.0$, the curve passes

Table 4b Comparison of experimental readings with computer model predictions (case 2, Suntech-3, at x = 19.0 cm)

Filter no.	Experimental readings, W/m^2, q_D ($\pm$ 100)	Predicted values, W/m^2, q_D	Discrepancy, %
F0	0	230	—
F1	1910	2036	+ 24
F2	1800	2070	+ 15
F3	3280	3310	+ 1
F4	3040	3030	0
F5	7500	7540	+ 1
F6	8520	8480	− 1
F7	12020	11930	0
Total spectrum	—	20370	—
rms (F3–F7)	—	—	1

Note: Inputs for gas and soot: T_g = 2085 K, T_s = 1865 K, t_s = 0.0018.

Table 4c Comparison of experimental readings with computer model predictions (case 3, JP-4, at x = 19.0 cm)

Filter no.	Experimental[a] readings, W/m^2, q_D ($\pm$ 100)	Predicted values, W/m^2, q_D	Discrepancy, %
F0	0	1280	—
F1	6070	6160	+ 1
F2	3950	3950	0
F3	5490	5580	+ 2
F4	4790	4710	− 2
F5	6890	6890	0
F6	9040	9050	0
F7	23460	22970	− 2
Total spectrum	—	27630	—
rms (F1–F7)	—	—	1.3

Note: Inputs for gas and soot: T_g = 1815 K, T_s = 2035 K, t_s = 0.0105.
[a]Readings were corrected to account for the purge air effect.

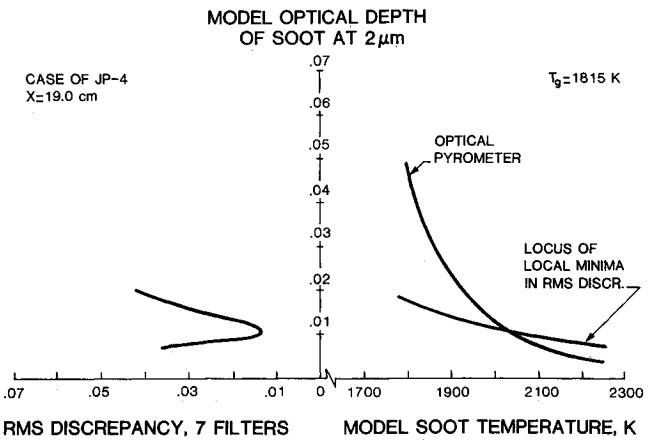

Fig. 11 Indicated optical depth of soot vs indicated soot temperature, JP-4.

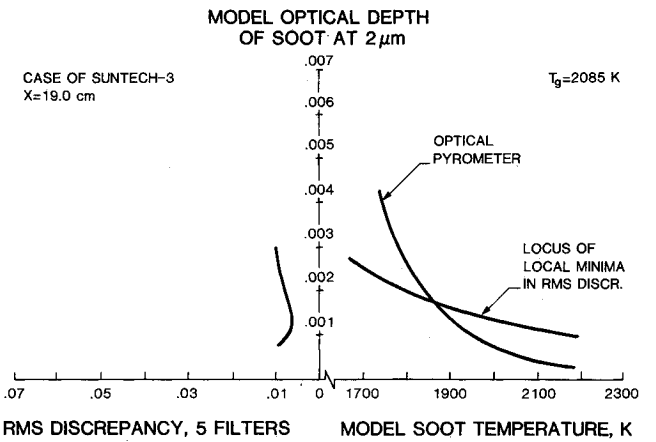

Fig. 12 Indicated optical depth of soot vs indicated soot temperature, Suntech-3.

within 5 K of the 2035 K effective soot temperature indicated by the filter readings.

Based on values of K_o = 1775 m^2/kg (Ref. 12), U = 25 m/s (Ref. 13), and the hydrogen-carbon fuel ratio and flame diameter in Tables 2 and 3, the fuel carbon present as soot at the axial station investigated is indicated to be 0.8%, in agreement with the 1% order of magnitude value given by Bard and Pagni.[14]

For the case of the Suntech-3 flame, filter readings F1 and F2 had to be disregarded because of too little soot radiation. When little or no soot is present, F1 and F2 readings cannot be interpreted because the filter transmittance cutoff wavelength is within the 2.7-μm CO_2 and H_2O overlapped bands. The filters were modeled based on spectral transmittance curves obtained at ambient temperature. During data collection, the cutoff wavelength changes slightly owing to filter heating. This change made low readings of F1 and F2 unreliable for both the Iso-Tet and Suntech-3 flames. Without reliable F1 and F2 predictions, the rms discrepancy does not have a deep minimum on which to rely in assigning t_s and T_s. However, the intersection of the locus of the rms minima and the optical pyrometer curve shown in Fig. 12 did permit an assignment of soot optical depth and temperature to be made, even though the amount of soot was only one-tenth that of the JP-4 flame. Tables 4b and 4c summarize the results for the Suntech-3 and JP-4 flames.

Conclusions

Filtered total radiometer measurements are seen to be convenient because of the simplicity, durability, and low cost

of the instruments. The 4.3-μm CO_2 band filter F5 gives a good indication of gas temperature when composition and path length are known.

In a flame with an optical depth of soot t_s at 2.0 μm equal to 0.0105, a sharp minimum was seen in the rms discrepancy between the seven filter readings and the model predictions, and it was possible to assign effective values of gas temperature, soot temperature, and soot optical depth based on the filtered radiometer readings. Even with a flame having one-tenth as much soot, the assignments were possible with the help of an optical pyrometer observation.

Direct observations of 1.1-1.4-μm wavelengths showed no indication of electronic band system emission. Conventional engineering correlations[10] were sufficient to predict the observed radiometer readings of the three flames.

Acknowledgments

This study is supported by the Naval Air Propulsion Center (NAVY contract N000140-8635-C-9151, G.S. Samuelsen, Principal Investigator). The United States Government is authorized to reproduce and distribute reprints for governmental purposes notwithstanding any copyright notation hereon. The authors gratefully acknowledge Dr. Larry Vickery in making a Cary 17D spectrophotometer available when needed, the assistance of Craig Wood and Roger Rudoff in operating the combustor, and Verna Bruce and Janice Johnson in preparing the manuscript.

References

[1]Marsland, J., Odgers, J., and Winter, J., "The Effects of Flame Radiation on Flame-Tube Metal Temperature," *Twelfth Symposium (International) on Combustion,* Vol. 12, 1969, The Combustion Institute, Univ. of Michigan, Ann Arbor, pp. 1265-1276.

[2]Lefebvre, A.H., "Flame Radiation in Gas Turbine Combustion Chambers," *International Journal of Heat and Mass Transfer,* Vol. 27, 1984, pp 1493-1510.

[3]Gaydon, A.G. and Wolfhard, H.G., *Flames, Their Structure, Radiation and Temperature,* 4th ed., Chapman and Hall, London, 1979.

[4]Tien, C.L. and Lee, S.C., "Flame Radiation," *Progress in Energy and Combustion Science,* Vol. 8, 1982, pp 41-59.

[5]Herzberg, G., *Molecular Spectra and Molecular Structure,* Van Nostrand Reinhold, New York, 1950.

[6]Wood, C.P., Smith, R.A., and Samuelsen, G.S., "Spatially-Resolved Measurements of Soot Size and Population in a Swirl-Stabilized Combustor," *Twentieth Symposium (International) on Combustion,* Vol. 20, 1984, pp. 1083-1094.

[7]Wood, C.P., Smith, R.A., and Samuelsen, G.S., "Optical Measurements of Soot Size and Number Density in a Spray-Atomized, Swirl-Stabilized Combustor," *ASME Journal of Engineering for Gas Turbines and Power,* Vol. 107, 1985, pp. 38-47.

[8]Gaydon, A.G., *The Spectroscopy of Flames,* 2nd ed., Chapman and Hall, London, 1974.

[9]Penner, S.S., *Quantitative Molecular Spectroscopy and Gas Emissivities,* Addison-Wesley, Reading, MA, 1959.

[10]Edwards, D.K., "Molecular Gas Band Radiation," *Advances in Heat and Mass Transfer,* Vol. 12, Academic Press, Orlando, FL, 1976, pp. 115-193.

[11]Edwards, D.K., *Radiation Heat Transfer Notes,* Hemisphere, New York, 1981.

[12]Lee, S.C. and Tien, C.L., "Optical Constants of Soot in Hydrocarbon Flames," *Eighteenth Symposium (International) on Combustion,* Vol. 18, 1981, pp. 1159-1166.

[13]Smith, R.A., Wood, C.P., and Samuelsen, G.S., "The Development and Use of a Surrogate Fuel to Simulate the Sooting Performance of a Practical Fuel," presented at Western States Section Meeting of the Combustion Institute, Davis, CA, Oct. 1985; also *Journal of Propulsion and Power* (submitted for publication).

[14]Bard, S. and Pagni, P.J., "Carbon Particulate in Small Pool Fire Flames," *Journal of Heat Transfer,* Vol. 103, 1981, pp. 357-362.